



Gruppo Nazionale di Geofisica della Terra Solida

# Atti del 38° Convegno Nazionale

12 - 14 NOVEMBRE 2019

ROMA - CONSIGLIO NAZIONALE DELLE RICERCHE



<b>EAGE</b> <small>EUROPEAN ASSOCIATION OF GEOSCIENTISTS &amp; ENGINEERS</small>	 <b>SEG</b> <small>SOCIETY OF EXPLORATION GEOPHYSICISTS</small>
<b>SEZIONE ITALIANA</b>	
19° CONVEGNO NAZIONALE	



Con il contributo di



ISTITUTO NAZIONALE DI  
OCEANOGRAFIA E DI  
GEOFISICA SPERIMENTALE



Consiglio Nazionale  
delle Ricerche



PROTEZIONE CIVILE  
Presidenza del Consiglio dei Ministri  
Dipartimento della Protezione Civile



ISTITUTO NAZIONALE DI  
GEOFISICA E VULCANOLOGIA

**EAGE**

EUROPEAN  
ASSOCIATION OF  
GEOSCIENTISTS &  
ENGINEERS

**SEG**

SOCIETY OF EXPLORATION  
GEOPHYSICISTS

**SEZIONE ITALIANA**

**19° CONVEGNO NAZIONALE**

Con la sponsorizzazione di



**CODEVINTEC**

Tecnologie per le Scienze della Terra e del Mare

- Lardeaux J.-M.; 2014: *Deciphering orogeny: a metamorphic perspective. Examples from European Alpine and Variscan belts. Part II: Variscan metamorphism in the French Massif Central – A review*. Bull. Soc. géol. France, **185(5)**, 281-310.
- Lardeaux J.-M., Schulmann K., Faure M., Janousek V., Lexa O., Skrzypek E., Edel J.B. and Stipska P.; 2014: *The Moldanubian Zone in the French Massif Central, Vosges/Schwarzwald and Bohemian Massif revisited: differences and similarities*. Geological Society of London, Special Publications, **405**, 7-44.
- Marotta A.M. and Spalla M.I.; 2007: *Permian-Triassic high thermal regime in the Alps: Result of late Variscan collapse or continental rifting? Validation by numerical modeling*. Tectonics, **26(4)**, 1-30.
- Matte P.; 2001: *The Variscan collage and orogeny (480-290 Ma) and the tectonic definition of the Armorica microplate: A review*. Terra Nova, **13(2)**, 122-128.
- Regorda A., Roda M., Marotta A.M. and Spalla M.I.; 2017: *2-D numerical study of hydrated wedge dynamics from subduction to post-collisional phases*. Geophysical Journal International, **211**, 974-1000.
- Roda M., Regorda A., Spalla M.I. and Marotta A.M.; 2019: *What drives Alpine Tethys opening? clues from the review of geological data and model predictions*. Geological Journal, **54(4)**, 2646-2664.
- Spalla M.I., Zannoni D., Marotta A.M., Rebay G., Roda M., Zucali M. and Gosso G.; 2014: *The transition from Variscan collision to continental break-up in the Alps: Insights from the comparison between natural data and numerical model predictions*. Geological Society, London, Special Publications, **405(1)**, 363-400.
- von Raumer J. F., Stampfli G.M. and Bussy, F.; 2003: *Gondwana-derived microcontinents – the constituents of the Variscan and Alpine collisional orogens*. Tectonophysics, **365**, 7-22.

## GOCE BAYESIAN GRAVITY INVERSION FOR GEONEUTRINO EXPLOITATION AT JUNO

L. Rossi<sup>1</sup>, V. Strati<sup>2,3</sup>

<sup>1</sup> Politecnico di Milano, Department of Civil and Environmental Engineering DICA, Milan, Italy

<sup>2</sup> University of Ferrara, Department of Physics and Earth Sciences, Ferrara, Italy

<sup>3</sup> INFN, Ferrara Section, Ferrara, Italy

**Introduction.** While the geophysical structure of the Earth is quite well known, information on its composition relies on shallow drill cores and samples brought to the surface by volcanic eruptions. Breakthroughs in the field are expected from the interplay between Earth Science and Particle Physics, which are currently exploring the promising scenarios of the Earth spectrometry with atmospheric neutrino oscillations (Rott *et al.*, 2015) and geoneutrinos detection (Fiorentini *et al.*, 2007). Geoneutrinos are a unique probe of the inaccessible deep Earth: by measuring their flux and energy spectrum it is possible to infer the global amount, distribution and ratio of U and Th, essential ingredients for the discrimination among different bulk silicate Earth (BSE) compositional models.

The recent measurements from Borexino (Italy) and KamLand (Japan) detectors are opening the way to multiple-sites geoneutrino studies aimed at distinguishing between the site-dependent crustal components (~75% of the signal) from the almost constant mantle component (~25% of the signal). Moreover, new geoneutrino measurements are highly awaited from the SNO+ detector (Canada) and from the Jiangmen Underground Neutrino Observatory (JUNO) experiment. However, to correctly discriminate the mantle contribution to the geoneutrino flux from the crustal one, geophysical and geochemical models in the surrounding of the detector are required. Currently, this task is mainly performed by exploiting global models, like CRUST 1.0, but site-specific models with local inputs can improve the accuracy of separation.

The goal of this work is to build a 3D geophysical model of the 6° × 4° area centred at the location of the JUNO experiment, currently under construction in the Guangdong Province (South China), by exploiting GOCE gravity data integrated with some a-priori geological and geophysical knowledge by means of a Bayesian approach to gravity inversion (Mosegaard and Tarantola, 2002).

In the following we analyse the provided geological and geophysical information, the inversion algorithm and the obtained results.

**Study area and available geophysical information.** The study area includes the northern margin of the South China Sea, the Guangdong region and the south-eastern part of Guangxi region. It is a part of the South China Block that has a complex tectonic history (John *et al.*, 1990), as well as poorly understood crustal composition and thickness (Zheng and Zhang, 2007).

As our final model assumes a layered crust and a one-layer uppermost mantle, we define the following surfaces: the topography/bathymetry, the bottom of sediments (i.e. the Top of the Upper Crust, TUC), the Top of the Middle Crust (TMC), the Top of the Lower Crust (TLC), the Moho Discontinuity (MD).

The constraints for the definition of the crustal model are obtained from published studies, including Deep Seismic Sounding profiles (DSS), Receiver Functions (RF), teleseismic P-wave velocity models and Moho depth maps, as shown in Fig. 1. Each of this data is taken according to its accuracy when introduced as prior probability in the Bayesian inversion algorithm.

**Bayesian gravity inversion.** We introduce an algorithm based on a Bayesian approach (Rossi *et al.*, 2016) and able to invert the gravity field by integrating some a-priori data on the crustal structure coming from geological and geophysical data. This approach allows obtaining a 3D voxel-wise crustal model beneath the detector.

The investigated volume is split into voxels,  $V_i$ , with index  $i = 1, 2, \dots, N$ . Each voxel is a regular prism with a fixed size and described by two parameters: a label  $L_i$ , denoting the material

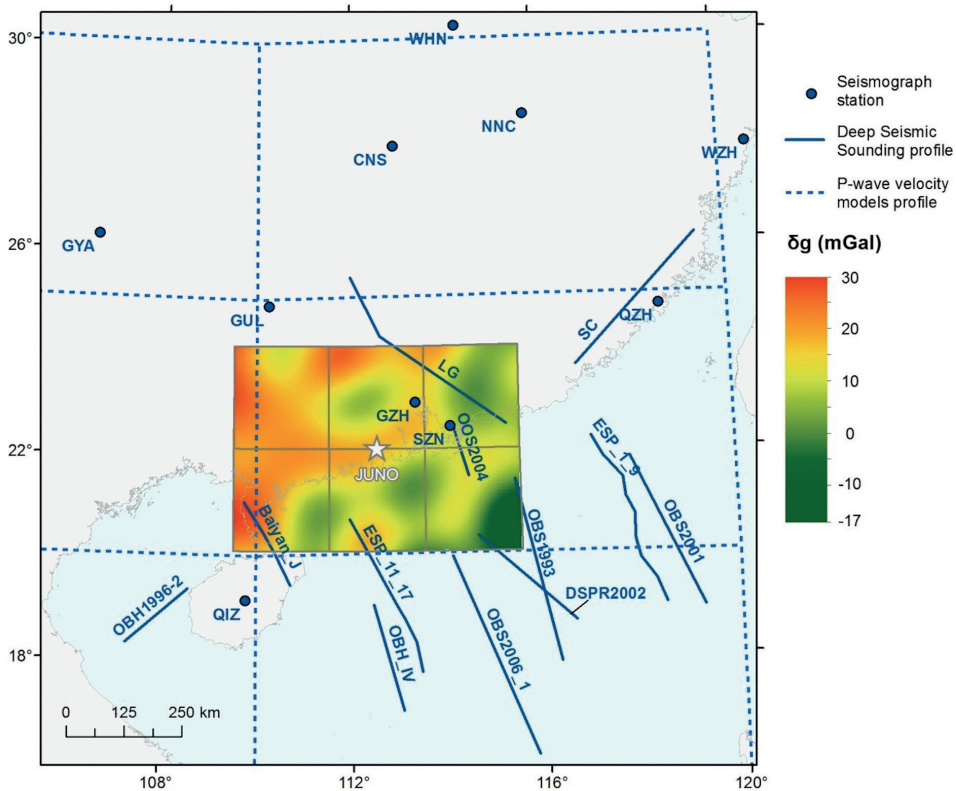


Fig. 1 - Geophysical input data used for the construction of the 3D model in the  $6^\circ \times 4^\circ$  area centred at the location of JUNO detector (Guangdong, South China) Data from deep seismic sounding profiles, P-wave velocity profiles and seismograph stations are used as input to build the a priori model for the inversion of gravimetric data. The raw observations of gravimetric disturbances ( $\delta g$ ) are represented as a continuous grid with  $5 \text{ km} \times 5 \text{ km}$  resolution.

inside the voxel (e.g. Upper Crust), and a mass density  $\rho_i$ . The prisms are disposed on a regular grid in Cartesian coordinates, and the forward modelling is performed in planar approximation. This geometry allows to easily introduce neighbourhood relationships. The inversion algorithm is based on the Bayes theorem:

$$P(x|y) \propto \mathcal{L}(y|x) P(x) \tag{1}$$

where  $y$  is the vector of observables, i.e. the gravity signal,  $x$  is the vector of parameters  $L$ ,  $\rho$  for all voxels,  $P(x|y)$  and  $P(x)$  are the posterior and the prior distribution, respectively, and  $\mathcal{L}(y|x)$  is the likelihood. Gravity is observed, therefore the likelihood represents the degree of fit between the observed and modelled signal. The prior distribution is defined by considering the available geological and geophysical information on the study region, integrated with some regularization conditions. This information is supplied to the algorithm in the following way:

- a range of variation of each boundary surface between two layers with different labels;
- neighbourhood rules between the possible couple of labels;
- the density of each material, i.e. of each label, in terms of the most probable value and its range of variation;
- constraints on lateral and vertical variation of the density (e.g. maximum admissible lateral and vertical variation or increasing/decreasing density with depth).

The shape of the prior distribution is chosen to highlight the dependency of each density  $\rho_i$  on the label  $L_i$ :

$$P(x) = \prod_{i=1}^N P(\rho_i|L_i) \cdot P(L_1, L_2, \dots, L_N) \tag{2}$$

The density of each voxel  $\rho_i$  is assumed to be normally distributed once the label  $L_i$  is given. Its mean  $\mu_\rho(L_i)$  and its variance  $\sigma_\rho^2(L_i)$  are given as a-priori information. Furthermore, the distribution is truncated at  $\mu_\rho(L_i) \pm 3 \sigma_\rho^2(L_i)$ , or even with a stricter range when required to satisfy the constraints.

On the other hand, the labels  $L$  are modelled as a Markov Random Field. Therefore, their probability distribution assumes the shape of a Gibbs distribution where the energy is the sum of the clique potential (Azencott, 1988), depending from two penalty functions  $s_i^2(L_i)$  and  $q^2(L_i, L_j)$ , where  $L_j$  is the label of a neighbour voxel. These functions are used to define the limits of the boundary surfaces and the neighbour rules between different materials, respectively. Moreover,  $q^2(L_i, L_j)$  inherently imposes the regularity of the boundary surfaces between two layers.

Then, invoking the Maximum A Posteriori (MAP) principle, the most probable set of labels and densities is chosen as the solution. This corresponds to find the minimum of the following target function:

$$F(\rho, L|y_o) = [y_o - y(x)]^T C_{vv}^{-1} [y_o - y(x)] + \eta \sum_{i=1}^N \frac{(\rho - \mu_\rho(L_i))^2}{\sigma_\rho^2(L_i)} + \gamma \sum_{i=1}^N s_i^2(L_i) + \lambda \sum_{i=1}^N \sum_{j \in \Delta_i} q^2(L_i, L_j) \tag{3}$$

conditioned to the constraints defined by prior information (e.g. maximum lateral density variation). Where  $y_o$  is the vector of observed gravity,  $C_{vv}^{-1}$  its noise covariance matrix and  $\eta$ ,  $\gamma$ , and  $\lambda$  weights balancing the contribution of the prior terms among them and with respect to the likelihood.

The minimum of Eq. 3 is retrieved by using a stochastic optimization method, i.e. a Simulated Annealing aided by a Gibbs Sampler (Robert and Casella, 2004).

**Gravity data and prior modelling.** The model to be estimated was chosen with a horizontal resolution of 50 km  $\times$  50 km and a vertical one of 100 m. The observations to be inverted are the gravity anomalies synthesized from the GOCE-only space-wise model up to degree and order 330 (Gatti and Reguzzoni, 2017). We choose this model since a satellite-only solution can avoid the introduction of useless high frequencies that cannot be interpreted by a voxel model with the given geometrical resolution.

The geophysical inputs explained in Sect. 2 are used to define the prior distribution in Eq. 2, providing geometrical and density information. Note that all the voxels above the TUC surface have fixed label and density because topography and bathymetry were taken from the GEBCO08 1' grid, while the sedimentary layers were taken from the CRUST 1.0 model.

The a-priori geometrical information entered as the admissible depth ranges of the TMC, TLC and Moho surfaces, computed by using the available geophysical data and their uncertainties and used to set up the penalty functions  $s_i^2(L_i)$  and  $q^2(L_i, L_j)$  in Eq. 3. In the areas lacking in local seismic information, an additional input was given by the global crustal model at  $1^\circ \times 1^\circ$  spatial resolution reported in Huang *et al.* (2013).

As for the a-priori probability distribution of the model density, the mean and standard deviation of Upper Crust (UC), Middle Crust (MC) and Lower Crust (LC) are defined reproducing the statistics of the CRUST 1.0 global values, integrated with local values inferred from DSS seismic velocity data, while the uppermost mantle layer is designed with a mean density according to the PREM model. To introduce a density spatial regularization in the final model, constraints on the maximum lateral and vertical variations between two adjacent voxels are introduced, under the condition of increasing or decreasing density with depth.

**Estimated crustal model.** The final estimation of the model is retrieved by optimizing the target function of Eq. 3 for different sets of input parameters. A set of  $10^3$  combination of the deterministic parameters present in Eq. 3, i.e. the ones weighting the prior terms and controlling the strength of the geometry and density constraints, are used to compute different solutions.

Then, to find the best one, a direct comparison of the target function values is not useful, because of the missing normalization. Therefore, four indexes are defined and computed per each estimated solution to evaluate the quality of gravity fitting, the level of density smoothing (considering both lateral and vertical variation) and the level of discontinuity surfaces smoothing. The best solution is chosen by a two-step procedure:

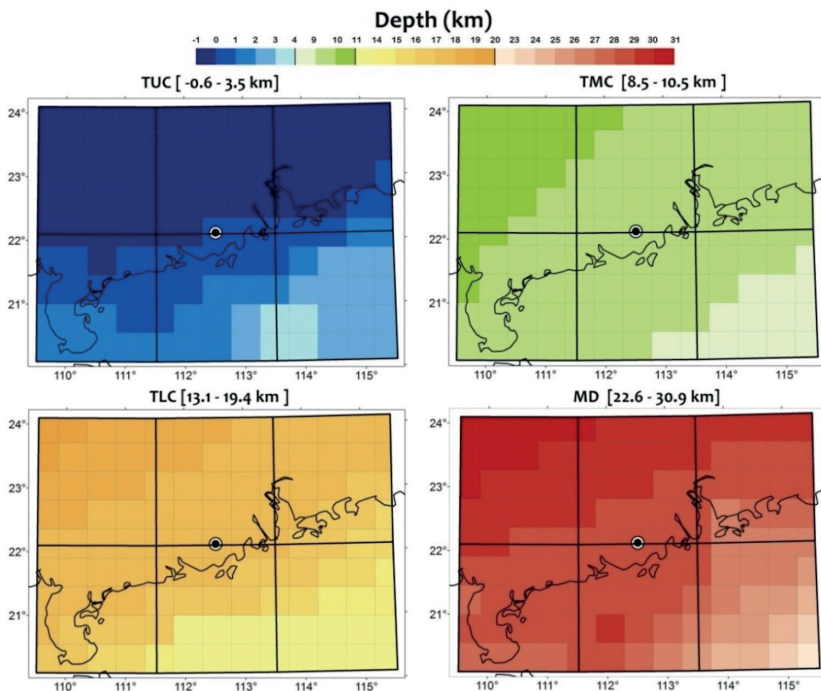


Fig. 2 - Depth maps of the Top of the Upper Crust (TUC), Top of the Middle Crust (TMC), Top of the Lower Crust (TLC) and Moho Discontinuity (MD) for the  $6^\circ \times 4^\circ$  area centred at the JUNO detector location. Negative values mean surfaces above the zero-level.

1. the solutions are filtered by imposing constraints on the values of the indexes, thus filtering 17 solutions among the  $10^3$  computed;
2. the one which vector of the indexes has the minimum norm has been chosen.

From now on, this model is called GIGJ (GOCE Inversion for Geoneutrinos at JUNO). The output of the GIGJ solution is made up of  $\sim 46 \times 10^3$  voxels, each one assigned with density and label values. Its geometry and density distributions are shown in Fig. 2 and Fig. 3, respectively. As expected, the GIGJ crustal model exhibits a crustal thinning moving from the north west (continental crust) to south-east (oceanic crust), together with a higher spatial heterogeneity of the UC density with respect to the MC and LC layers.

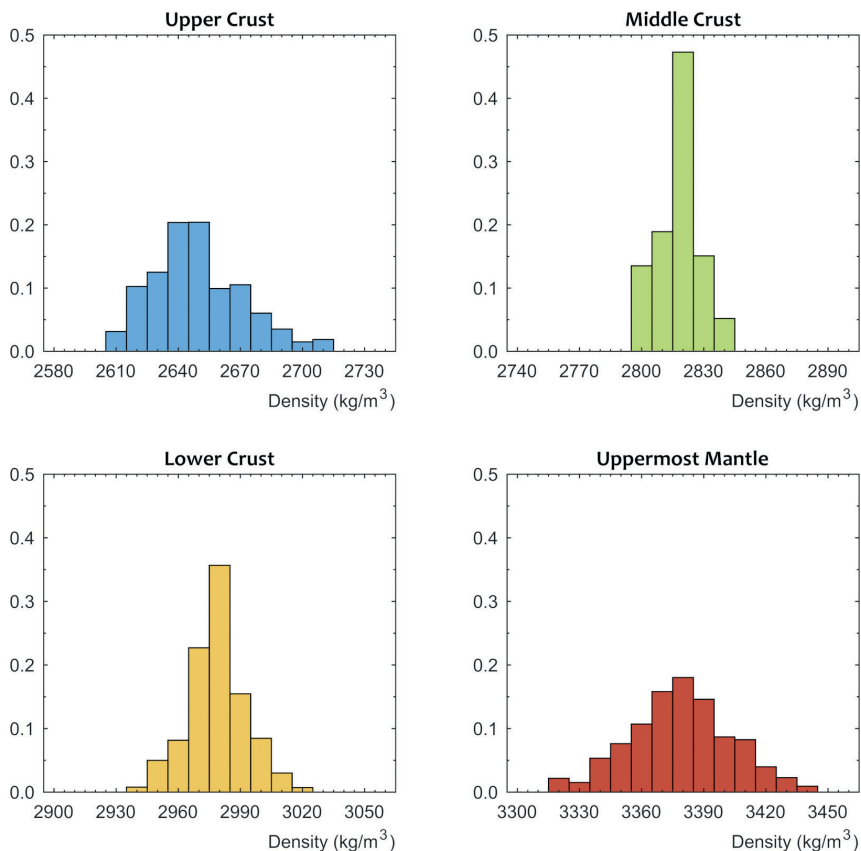


Fig. 3 - Frequency distributions of the density values for each label of the GIGJ model for the Upper Crust, Middle Crust, Lower Crust and Uppermost Mantle. The latter corresponds to the portion of continental lithospheric mantle down to a constant depth of 50 km.

With the aim of estimating the geophysical contribution to the geoneutrino signal uncertainty for each crustal layer, the overall mass and volume uncertainty of the GIGJ solution was calculated. It comprises an estimation error component associated to the solution of the inverse gravimetric problem and a systematic error component due to the adoption of a fixed sedimentary layer. Since the joint posterior distribution  $P(\rho, L | y_o)$  of all the voxels cannot be evaluated, the estimation error component of GIGJ was split into a density and a geometry contribution, both estimated by sample statistics on proper marginal distributions of the individual voxels.

**Expected geoneutrino signal.** The GIGJ model was divided into  $7 \times 10^7$  cells of  $1 \text{ km} \times 1 \text{ km} \times 0.1 \text{ km}$ , each one assigned with crustal layer label, density value and unitary U and Th

abundances ( $\alpha_U = \alpha_{Th} = 1 \mu\text{g/g}$ ). The expected geoneutrino signal linearly scales with the U and Th mass distributed in the crust and depends on the source-detector distance  $r$  by a combined effect of the  $1/4\pi r^2$  spherical scaling factor and the average antineutrino survival probability, which oscillations gradually damp for increasing distance from the experimental site. Based on the approach and input parameters described in Sect. 7 of Strati *et al.* (2017), we calculated the geoneutrino signal expressed in Terrestrial Neutrino Units (TNU) (Fiorentini *et al.*, 2007).

From the comparison between the signals calculated using the prior and GIGJ models, it is possible to infer that the benefit of using gravity information with the proposed inversion procedure, led to a site-specific repartition of the signal contribution from deep layers (MC and LC) together with their uncertainty.

**Conclusions.** GIGJ is a 3D numerical model constituted by  $\sim 46 \times 10^3$  voxels of  $50 \times 50 \times 0.1$  km. GIGJ fitted homogeneously distributed GOCE gravity data with a standard deviation of the residuals of the order of 1 mGal, compatible with the observation accuracy. The solution was the smoothest one in terms of both density distribution and geometrical shape.

Regarding geoneutrino signals prediction, the main outcome of this study was the 77%, 55% and 78% reduction of the UC, MC and LC signal uncertainty. Because of the rearrangement of the crustal layers thicknesses, we predicted a reduction ( $\sim 21\%$ ) and an increase ( $\sim 24\%$ ) of the MC and LC signal respectively, in comparison with the results obtained from global models.

This study demonstrated that a Bayesian-based gravimetric inversion applied to reliable satellite data, rationally integrated with local geological and seismic information, provided a coherent picture of the crustal structure at the natural spatial scale required for geoneutrino studies.

**Acknowledgements.** We would to thanks M. Reguzzoni, M. Baldoncini, I. Callegari, P. Poli, D. Sampietro and F. Mantovani for the support to the research and the JUNO Italian Collaboration for the useful reviews and comments

## References

- Azencott R (1988). Simulated annealing. Séminaire Bourbaki (1987-1988), 30, 223-237.
- Fiorentini G, Lissia M, and Mantovani F (2007). Geo-neutrinos and earth's interior. Phys. Rep., 453(5-6), 117-172.
- Gatti A and Reguzzoni M (2017). GOCE gravity field model by means of the space-wise approach (release R5). GFZ Data Services.
- Huang Y, Chubakov V, Mantovani F, Rudnick RL, and McDonough WF (2013). A reference Earth model for the heat-producing elements and associated geoneutrino flux. Geochem., Geophys., Geosyst., 14(6), 2023-2029.
- John BM, Zhou XH, and Li JL (1990). Formation and tectonic evolution of Southeastern China and Taiwan: Isotopic and geochemical constraints. Tectonophysics, 183(1-4), 145-160.
- Mosegaard K and Tarantola A (2002). Probabilistic approach to inverse problems. Int. Geophys., 81, 237-265.
- Robert CP and Casella G (2004). Monte Carlo Statistical Methods.
- Rossi L, Reguzzoni M, Sampietro D, and Sansò F (2016). Integrating geological prior information into the inverse gravimetric problem: the Bayesian Approach. In N Sneeuw, P Novák, M Crespi, & F Sansò (Eds), VIII Hotine-Marussi Symposium on Mathematical Geodesy: Proc. of the Symposium in Rome, 17-21 June, 2013 (pp. 317-324). Cham: Springer Int. Pub.
- Rott C, Taketa A, and Bose D (2015). Spectrometry of the Earth using Neutrino Oscillations. Sci. Rep., 5, 15225.
- Strati V, Wipperfurth SA, Baldoncini M, McDonough WF, and Mantovani F (2017). Perceiving the Crust in 3-D: A Model Integrating Geological, Geochemical, and Geophysical Data. Geochem., Geophys., Geosyst., 18(12), 4326-4341.
- Zheng Y and Zhang S (2007). Formation and evolution of Precambrian continental crust in South China. Chin. Sci. Bull., 52(1), 1-12.